Photodissociation Dynamics of Thiophenol-d_1: The Nature of Excited Electronic States along the S−D Bond Dissociation Coordinate

Jeong Sik Lim, Heechol Choi, Ivan S. Lim,[†] Seong Byung Park,[‡] Yoon Sup Lee,* and Sang Kyu Kim*

Department of Chemistry, KAIST, Daejeon (305−701), Republic of Korea

Received: August 10, 2009

The S−D bond dissociation dynamics of thiophenol-d_1 (C_6H_5SD) pumped at 266, 243, and 224 nm are examined using the velocity map ion imaging technique. At both 266 and 243 nm, distinct peaks associated with $\tilde{X}$ and $\tilde{A}$ states of the phenylthiyl radical ($C_6H_5S\cdot$) are observed in the D^+ image at high and low kinetic energy regions, respectively. The partitioning of the available energy into the vibrational energy of the phenylthiyl radical is found to be enhanced much more strongly at 266 nm compared to that at 243 nm. This indicates that the $\pi\pi^*$ electronic excitation at 266 nm is accompanied by significant vibrational excitation. Given the relatively large anisotropy parameter of -0.6, the S−D dissociation at 266 nm is prompt and should involve the efficient coupling to the upper-lying $n_\pi\sigma^*$ repulsive potential energy surface. The optical excitation of thiophenol at 224 nm is tentatively assigned to the $\pi\sigma^*$ transition, which leads to the fast dissociation on the repulsive potential energy surface along the S−D coordinate. The nature of the electronic transitions associated with UV absorption bands is investigated with high-level ab initio calculations. Excitations to different electronic states of thiophenol result in unique branching ratios and vibrational excitations for the fragment of the phenylthiyl radical in the two lowest electronic states.

I. Introduction

Recently, the presence of the $\pi\sigma^*$ state nearby the closely-lying $\pi\pi^*$ state and its essential role in the electronic dephasing process have been spotlighted both theoretically and experimentally for many aromatic compounds having XH moieties (X = N, O, S) such as phenol,[1–6] thiophenol,[7–9] pyrrole,[10–20] imidazole,[21] indole,[22–26] adenine,[27–42] and pyrimidines.[30,43–51] The $\pi\sigma^*$ electronic state is repulsive in nature along the X−H coordinate and correlates adiabatically or diabatically to the lower-lying electronic states. The optically dark $\pi\sigma^*$ state is thus considered to be one of the main pathways for the electronic dephasing of the nearby $\pi\pi^*$ excited state of some heteroaromatic compounds including biological building blocks such as adenine[27–42] and tryptophan-H$^+$.[52–56] The $\pi\sigma^*$ state has also been found to play a primary role in the solvent-assisted proton transfer reactions which are ubiquitous in chemistry and biology.[4,57–69] Accordingly, many experimental and theoretical studies have been focused on the dissociation dynamics of aromatic compounds in which $\pi\sigma^*$ and $\pi\pi^*$ states are strongly coupled. However, many intriguing dynamical questions concerning the multidimensional nature of the nonadiabatic transitions involved in the X−H dissociation seem to still be open. In particular, many studies had been focused on O−H or N−H bond dissociation dynamics, whereas S−H bond dissociation dynamics of aromatic compounds has been studied relatively little. Since the valence orbital of the atomic sulfur is 3p, the nature of the molecular orbital of the sulfur-containing aromatic compounds is expected to be somewhat different in terms of the extent to which the electronic delocalization occurs over

the entire molecule compared to the compounds containing valence 2p atoms such as O or N atoms. We have recently reported the study of the photodissociation dynamics of thiophenol.[7–9] The S−H bond dissociation resulting from the perpendicular transition is prompt and gives rise to the phenylthiyl radical ($C_6H_5S\cdot$) populated in its two closely lying ground ($\tilde{X}$) and first excited ($\tilde{A}$) electronic states. The energy difference between $\tilde{X}$ and $\tilde{A}$ states originates from the different orientations of the singly occupied molecular orbital (SOMO) with respect to the molecular plane. That is, the ground-state configuration gives SOMO aligned perpendicular to the molecular plane, while the first electronically excited state is characterized by the parallel orientation of the SOMO with respect to the molecular plane.[7–9] Thus, photodissociation of thiophenol generates so-called "the intramolecular orbital alignment", a novel concept in the field of stereochemistry. It is noteworthy that a number of theoretical studies on σ and π states of the phenoxyl radical ($C_6H_5O\cdot$), which can be obtained as a product from phenol dissociation, have focused on the control of the branching ratio resulting from a couple of nonadiabatic transitions along the reaction coordinate.[5,6] The experimental approach, however, seems to be nontrivial for phenol, since $\tilde{X}$ and $\tilde{A}$ states of the phenoxyl radical have a large energy gap, making it difficult to observe the significant contributions of both $\tilde{X}$ and $\tilde{A}$ products without losing the energy resolution. Since both $\tilde{X}$ and $\tilde{A}$ states of phenylthiyl radical are energetically accessible and separately observable in the D kinetic energy distributions, thiophenol provides an ideal system for the study of nonadiabatic couplings encountered in the exit channel. In our previous publications, we have concentrated on the dynamics of thiophenol at 243 nm.[7–9] Here, we report the dissociation dynamics of thiophenol-d_1 at two different wavelengths of 266 and 224 nm. Branching ratios, fragment vibrational excitations, and anisotropy parameters are measured to offer insights into

* Authors to whom correspondence should be addressed. sangkyukim@kaist.ac.kr (S.K.K.), yoonsuplee@kaist.ac.kr (Y.S.L.).
† ivanslim@gmail.com.
‡ Present address: Department of Chemistry, Seoul National University, Seoul, Korea.

the nature of the adiabatic or diabatic potential energy surfaces especially in terms of vibronic couplings along the dissociation coordinates.

II. Experimental Section

The experimental setup was described in detail in our earlier reports.[7,70] Briefly, thiophenol (Aldrich) was dissolved in ether and vigorously stirred with an excess amount of the D_2O solvent. Then, the C_6H_5SD-enriched thiophenol sample was extracted to give thiophenol-d_1. The sample was heated to 50 °C, mixed with He carrier gas, and expanded into vacuum through a nozzle orifice (General Valve 9 series, $\phi = 0.3$ mm) with a backing pressure of 3 atm. The supersonic jet was then skimmed through a 1-mm-diameter skimmer prior to being overlapped with the excitation laser pulse. The third harmonic output of a Nd:YAG laser (Spectra-Physics GR150) was used to pump a dye laser (Lambda Physik Scanmate 2) to generate the laser pulse at 243 or 224 nm after frequency doubling on a β-barium borate (BBO) crystal placed on a homemade autotracker. The fourth harmonic of the YAG laser was used to generate the 266 nm laser pulse with a broad bandwidth of $\sim$1 cm^{-1}. The polarization of the pump laser pulse was perpendicular to the time-of-flight axis and the molecular beam while it is parallel to the detection plane. The D fragment was detected either by the $(2 + 1)$ resonance-enhanced multiphoton ionization at 243 nm or by the $(1' + 2)$ two-color multiphoton ionization using laser pulses at 266 and 224 nm. In the former case, the laser frequency was scanned over the entire Doppler width to detect the D fragment distributed over the wide kinetic energy range. In the latter case, the Doppler-reduced ionization method proposed by the Suits group[71] was employed. The 266 and 224 nm laser pulses were overlapped in a counter-propagating way to detect the D fragment. Here, the Doppler shift caused by large velocity vector of the D fragment was fully covered with the broad bandwidth of the fourth harmonic output of the Nd:YAG laser.[71] The D fragment ions were velocity mapped onto a position-sensitive detector equipped with dual microchannel plates and a P20 phosphor screen (Burle, 3040 FM CT, 40 mm diameter). The image was taken via a charge-coupled device camera (Hammamatsu, C8800−01C) by the gravity event counting method to be averaged over 36 000 laser shots. Raw images were reconstructed using the basis-set expansion (BASEX) and/or Labview-based polar basis function expansion (LV_pBASEX) algorithms to give images for center slices of three-dimensional spatial distributions of the fragment.[72,73]

In the state-averaged complete active space self-consistent field (SA-CASSCF) calculations, a large active space, which is 12 electrons in 11 molecular orbitals (MOs), and the 6-311++G-(3df,3pd) basis set were used first. The three pairs of π/π^* orbitals of the benzene moiety, the n_p orbital on S, and the two pairs of σ/σ^* orbitals (σ_{CS}, σ^*_{CS}, σ_{SH}, and σ^*_{SH}) were included in this active space. Further calculations for dynamical correlation at the complete active space second-order perturbation theory (CASPT2) level with such a large active space demand a very expensive computational cost. In this work, therefore, the MOs, associated occupation numbers, and transition dipole moments for three lowest electronically excited states as well as the ground-state equilibrium geometry of thiophenol were obtained through the reduced active space (8,9) where the σ_{CS} and σ_{SH} orbitals were excluded from the aforementioned active space because the occupation numbers of both orbitals were close to 2, meaning that they do not play an important role in the nature of excited states. All states were given equal weighting in the SA-CASSCF(8,9) calculations. The final
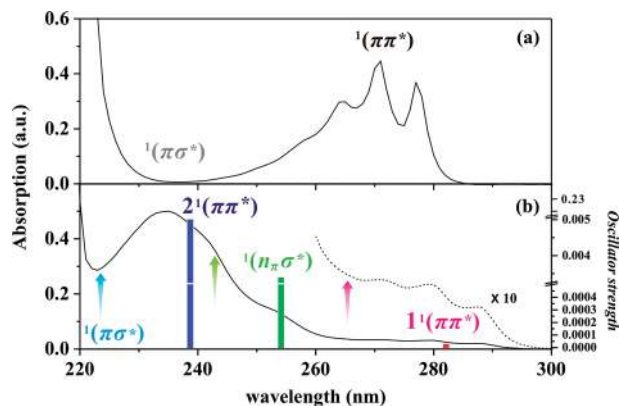

Figure 1. UV absorption spectra of (a) phenol and (b) thiophenol in *n*-hexanes. The region represented as dots in (b) is magnified by 10 times to show the diffuse but still resolved vibrational structure. Vertical arrows represent the pump wavelengths used in this work, whereas the calculated vertical excitation energies are depicted as sticks.

vertical excitation energies and associated oscillator strengths were calculated at the CASPT2 level with the SA-CASSCF(8,9) reference. This approach being one of the multireference-based methods is useful to describe the electronic and energetic properties of near-degenerate states and, accordingly, is favored here because three electronic states in the present system are very close in energy (see Figure 2). In previous theoretical works on the excited states of sulfur-containing molecules, it is shown that the calculated results at the CASPT2//CASSCF level are in better agreement with experimental ones than single-reference-based methods.[74,75] In ref 74, the average errors of the time-dependent density functional theory (TD-DFT) and the equation-of-motion coupled-cluster singles and doubles (EOM-CCSD) relative to the experimental excitation energies were quite a bit larger than CASPT2. In this work, the TD-DFT calculations were performed with the HCTH functional (TD-HCTH) and the same basis set, and the EOM-CCSD ones were done with the aug-cc-pVTZ basis set for comparison. The *Gaussian03*[76] program packages were used for TD-HCTH and the MOLPRO packages[77] for SA-CASSCF, CASPT2, and EOM-CCSD calculations.

III. Results and Discussion

It is quite intriguing to compare UV absorption spectra of thiophenol and phenol as shown in Figure 1. The most pronounced difference is the fact that thiophenol has a very strong absorption band peaked at $\sim$234 nm whereas phenol does not show any significant absorption band in the corresponding wavelength region. In contrast, the optical transition of phenol in the 260−280 nm range is quite strong and has been well-characterized as the $\pi\pi^*$ transition, while that of thiophenol in the same spectral range is diffuse in nature and has not been thoroughly characterized. This large difference in the absorption spectra of two molecules should come from the 3p character of the SH moiety in thiophenol compared to the 2p nature of the OH group in phenol. Our CASPT2 calculation gives the vertical excitation energies of 282 nm for the first $^1(\pi\pi^*)$ transition, 254 nm for the $^1(n_\pi\sigma^*)$ excitation, and 238 nm for the second $^1(\pi\pi^*)$ transition (Figures 1 and 2). The CASPT2 vertical excitation energies and the corresponding oscillator strengths describe the UV absorption spectrum of thiophenol quite well, significantly better than those from the TD-HCTH or the EOM-CCSD calculation (Figure 1 and Table 1). The current CASPT2 calculation seems to yield a much better description of the UV
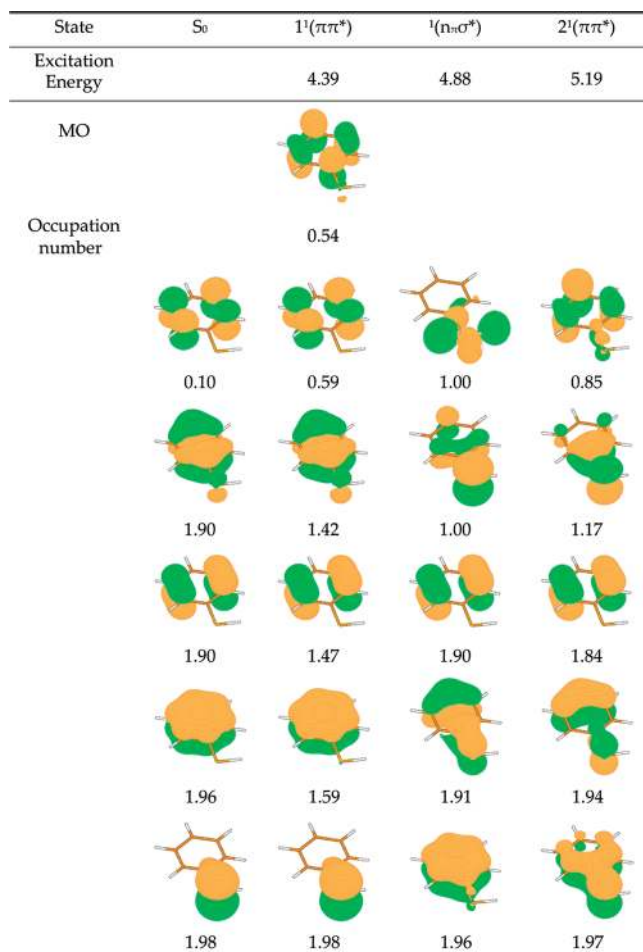
State	S₀	1¹(ππ*)	¹(nπσ*)	2¹(ππ*)
Excitation Energy		4.39	4.88	5.19

Figure 2. MO diagrams and associated occupation numbers for three lowest excited states of thiophenol at the SA-CASSCF(8,9) level. Excitation energies (in eV) are obtained at the CASPT2 level with SA-CASSCF(8,9) orbitals of the ground state.

It should be noted that the second $^1(\pi\pi^*)$ transition leaves two highest-occupied molecular orbitals partially filled (Figure 2), suggesting that the nonbonding orbital localized on sulfur is involved in the corresponding transition, and this in turn could be responsible for the lowering of the second $^1(\pi\pi^*)$ excitation energy compared to the previous calculation.[7,8] The relative oscillator strength of the first $^1(\pi\pi^*)$ transition compared to that of $^1(n_\pi\sigma^*)$ or the second $^1(\pi\pi^*)$ transition is calculated to be far below the experimental observation, casting some doubt over the reliability of theoretical oscillator strengths based on the CASPT2 level. This is particularly true for cases exhibiting avoided crossings. The discrepancy between experimental and calculated values might be reduced by inclusion of the vibrational-state dispersion accompanied by the optical transitions. Additionally, Rydberg characters of the optical transtions which are not considered in the present calculations may also be responsible for the discrepancy of the theory and the experiment.

At 243 nm, according to the present calculation (Figure 1 and Table 1), both $^1(n_\pi\sigma^*)$ and the second $^1(\pi\pi^*)$ states (S$_2$ and S$_3$) are optically accessible, with the latter possessing the higher transition probability. The experimental fact that the S–D bond dissociation at 243 nm is prompt,[7-9] however, indicates that the coupling to the lower-lying repulsive $^1(n_\pi\sigma^*)$ state of the initially prepared S$_3$ state should be very efficient, and this is consistent with the diffuse character of the UV absorption spectrum in the corresponding wavelength region. The D translational energy distribution at 243 nm, as reported in our earlier publications,[7-9] shows long tails at the low kinetic energy region indicating that the nascent phenylthiyl radical is vibrationally excited in both ground and excited states (Figure 3). Even after considering the impulsive force which would be localized on the S–D moiety in the photodissociation process, the torque exerted on the phenylthiyl moiety is expected to be very tiny because of the large mass difference between D and S. Therefore, the efficient vibrational energy transfer during the prompt S–D bond dissociation process is less likely. Rather, the structural change of thiophenol upon the optical transition should be largely responsible for the vibrational excitation of the phenylthiyl fragment. In other words, the vibrational excitation of thiophenol in the excited state for the vibrational modes orthogonal to the reaction coordinate may be conserved during the ultrafast S–D bond dissociation. It would thus be very intriguing if the vibrational structure involved in the optical excitation could be revealed in the vibrational excitation of the fragment in the case of the ultrafast bond rupture involving the light atom. DFT vibrational frequencies of the ground-state
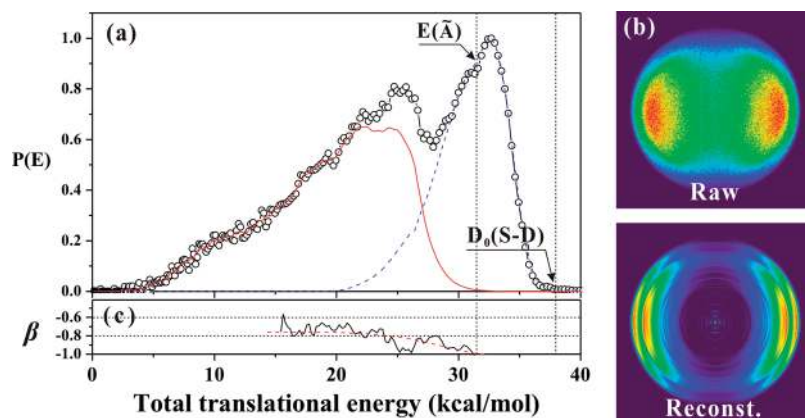
absorption spectrum than the previous one,[7,8] implying that multireference theoretical calculations probably require larger basis set and active space comparable to the present CASPT2// SA-CASSCF(8,9)/6-311++G(3df,3pd) level. The transition dipole moment of the $^1(n_\pi\sigma^*)$ transition calculated at the optimized geometry of the ground state is perpendicular to the molecular plane, whereas those of the first and second $^1(\pi\pi^*)$ transitions are on the molecular plane with angles of 53° and 83°, respectively, with respect to the S–D bond axis (Table 1).

TABLE 1: Calculated Vertical Excitation Energies Expressed in Wavelength, Oscillator Strengths, and Transition Dipole Moments

state	excitation wavelength (nm)	oscillator strength	transition dipole moment (μ)[a]		
			μ_x	μ_y	μ_z
		CASPT2//SA-CASSCF(8,9)/6-311++G(3df,3pd)			
1¹(ππ*)	282.18	3.1 × 10⁻⁵	−0.016	0.007	0.000
¹(nπσ*)	254.29	3.4 × 10⁻³	0.000	0.000	0.170
2¹(ππ*)	238.95	0.22	−1.329	0.006	0.000
		TD-HCTH/6-311++G(3df,3pd)			
1¹(ππ*)	284.63	9.8 × 10⁻³	−0.052	0.299	0.000
¹(nπσ*)	274.54	2.9 × 10⁻³	0.000	0.000	0.162
2¹(ππ*)	255.95	0.23	1.389	0.005	0.000
		EOM-CCSD/aug-cc-pVTZ//CCSD/cc-pVTZ			
1¹(ππ*)	254.69	4.5 × 10⁻³	−0.047	−0.188	0.000
¹(nπσ*)	238.80	3.2 × 10⁻³	0.000	0.000	0.158
2¹(ππ*)	214.36	0.23	1.292	0.004	0.000

[a] See the molecule-fixed axes defined in Figure 6.

Figure 3. Total translational energy distribution (a) of the fragmented D atom from thiophenol-d_1 at 243 nm photodissociation and (c) anisotropy parameters as a function of total translational energy (reproduced from ref 8). Raw ion image and the center slice of the reconstructed 3D distribution of the D fragment are shown in (b).

TABLE 2: DFT Vibrational Frequencies of the Ground-State Thiophenol-d_1 and Phenylthiyl Radical Obtained at the B3LYP/6-311++G(3df,3pd) level[a,b]

	thiophenol-d_1		phenylthiyl radical	
mode[c]	symmetry	frequency (cm^{-1})[d]	symmetry	frequency (cm^{-1})
τ	a″	97	disappearing mode	
10b	a″	181	b$_1$	161
15	a′	268	b$_2$	299
6a	a′	408	a$_1$	430
16a	a″	409	a$_2$	385
16b	a″	482	b$_1$	467
6b	a′	631	b$_2$	622
β	a′	689	disappearing mode	
4	a″	694	b$_1$	682
7a	a′	709	a$_1$	731
11	a″	754	b$_1$	775
10a	a″	849	a$_2$	853
17b	a″	917	b$_1$	955
17a	a″	988	a$_2$	1006
12	a′	991	a$_1$	997
5	a″	999	b$_1$	1012
1	a′	1043	a$_1$	1037
18b	a′	1103	b$_2$	1096
18a	a′	1110	a$_1$	1080
9b	a′	1183	b$_2$	1180
9a	a′	1208	a$_1$	1201
14	a′	1311	b$_2$	1299
3	a′	1354	b$_2$	1340
19b	a′	1472	b$_2$	1457
19a	a′	1511	a$_1$	1480
8b	a′	1610	b$_2$	1574
8a	a′	1624	a$_1$	1594
ν	a′	1934	disappearing mode	
20a	a′	3166	a$_1$	3171
7b	a′	3171	b$_2$	3181
13	a′	3182	a$_1$	3192
20b	a′	3187	b$_2$	3202
2	a′	3198	a$_1$	3205

[a] The MS group of the optimized thiophenol-d_1 and phenylthiyl radical is C_s and C_{2v}, respectively. [b] In the phenylthiyl radical, the C_2 axis is the x axis in Figure 6. [c] Normal modes are labeled according to ref 76. The symbol of τ, β, or ν means CCSD torsion, CSD bending, or SD stretching, respectively. [d] The modes are listed following the increasing order for the magnitude of thiophenol-d_1 frequencies.

thiophenol-d_1 and phenylthiyl radical obtained at the B3LYP/6-311++G(3df,3pd) level are listed in Table 2. The in-plane C−C−S bending calculated at 299 cm^{-1} for the ground phenylthiyl radical would be one of the plausible candidates
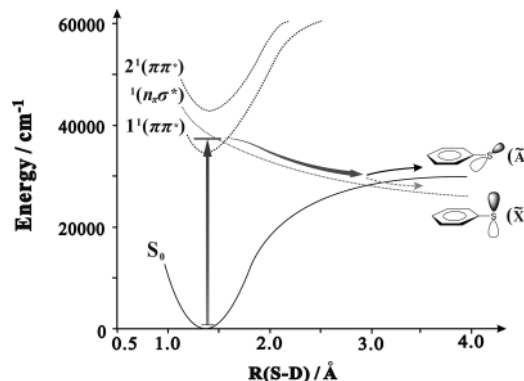

Figure 4. Simplified schematic diagram of the potential energy surface of thiophenol-d_1 as a function of the S−D distance at the planar geometry showing the plausible mechanism for the dissociation at 266 nm.

for the vibrational excitation mode associated with the $^1(n_\pi\sigma^*)$ and/or second $^1(\pi\pi^*)$ transition. The ab initio calculation for the minimum energy structure of the excited state with respect to all coordinates other than the repulsive S−D elongation coordinate would be highly desirable.

In the region where the upper A″ electronic state crosses the ground A′ electronic state at the planar geometry (the SH group is planar with the benzene moiety in the ground electronic state), the reaction flux bifurcates into either $\tilde{X}$ and $\tilde{A}$ state of the phenylthiyl fragment through the conical intersection induced by the vibronic mixing of upper and low diabatic states (Figure 4). At the pump energy of 243 nm, the $\tilde{A}/\tilde{X}$ branching ratio is experimentally estimated to be 1.31, showing the preference for the $\tilde{A}$ state at the asymptotic limit. In the case of the thiophenol dissociation at 243 nm, since the reaction undergoes directly or indirectly (via S$_3$) accessed $^1(n_\pi\sigma^*)$ state, which is repulsive along the S−H coordinate, the branching ratio is likely to be determined at the conical intersection between S$_0$ and S$_2$. The anisotropy parameter of $\beta = -0.76$ for the $\tilde{A}$ state of the phenylthiyl radical which is reduced from $\beta = -1$ for the $\tilde{X}$ state suggests that the adiabatic potential energy surface correlating to the $\tilde{A}$ state could involve the additional low-frequency vibrational excitation at the S$_2$/S$_0$ conical intersection.[7−9] Another possibility is that different anisotropy values for $\tilde{X}$ and $\tilde{A}$ states may originate from the different extent of coupling for the perpendicular and the nearly perpendicular transition dipole moments associated with the S$_2$−S$_0$ and S$_3$−S$_0$ transitions, respectively.
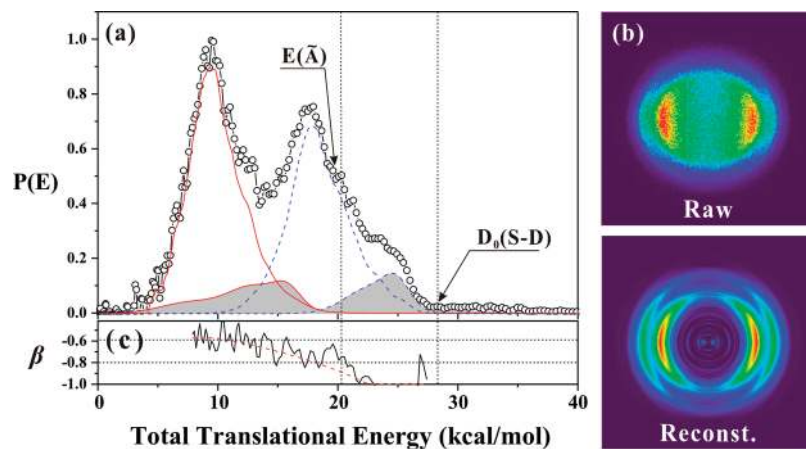
Figure 5. (a) Total translation energy distribution (○) of the fragmented D atom at 266 nm, which is deduced from (b) the raw and reconstructed images of D. In (c), anisotropy parameter is plotted as a function of total translational energy. The $\tilde{X}$ (dotted line) and $\tilde{A}$ state (solid line) of the phenylthiyl radical from the S_1–S_0 excitation is depicted after the deconvolution (see the text). The contribution from the direct photodissociation due to the S_2–S_0 excitation is shaded.

The D^+ image taken at the pump energy of 266 nm is quite different from that observed at 243 nm (Figure 5). As indicated in Figure 1, the 266 nm excitation is most likely due to the first $^1(\pi\pi^*)$ and $^1(n_\pi\sigma^*)$ transitions, with the latter of the lower transition probability (Table 1). Consistently, the D distribution in Figure 5 clearly shows a sharp shoulder at the high kinetic energy region. The limiting value of $\beta = -1$ measured for the shoulder at the high kinetic energy region indicates that the associated fragments should originate from the perpendicular transition. This assignment matches well with the absorption spectrum of thiophenol (Figure 1), since the absorption due to the $^1(n_\pi\sigma^*)$ transition starts to rise at around 266 nm while the vibrational progression of the $^1(\pi\pi^*)$ transition seems to be persistent in the corresponding energy region. Calculated vertical excitation wavelengths of 282 and 254 nm for the first $^1(\pi\pi^*)$ and $^1(n_\pi\sigma^*)$ transitions, respectively, also support this assignment (Table 1). It seems to be nontrivial to separate out the contributions of the $^1(n_\pi\sigma^*)$ and the S_1 transitions from the total kinetic energy distribution. It is assumed here that the shape of the kinetic energy distribution at 266 nm is identical to that at 243 nm. This is subject to the more fundamental assumption that dynamic constraints on the repulsive S_2 state are little dependent on the pump energy at least in the energy range 243–266 nm. The total kinetic energy distribution could then be deconvoluted as shown in Figure 5. Two distinct peaks at low and high kinetic energy regions are, similar to the 243 nm case, ascribed to the $\tilde{A}$ and $\tilde{X}$ states of phenylthiyl radical, respectively. The relatively large value of the apparent anisotropy parameter ranging from -0.6 to -0.8 indicate that the dissociation is prompt and two transition dipole moments of the first $^1(\pi\pi^*)$ and $^1(n_\pi\sigma^*)$ transitions, of which the tilt angles with respect to the S–D bond axis are calculated to be 53° and 90°, respectively, should contribute to the observed anisotropic distribution of the final products (Table 1 and Figure 6). The initial S_1 state reached by the $^1(\pi\pi^*)$ transition should be efficiently coupled to the repulsive S_2 state leading to the prompt S–D dissociation. The coupling of S_1 to S_2 may occur through a vibronic coupling aided by the odd-quanta excitation of the out-of-plane mode in S_2 because of the symmetry conservation. At 266 nm where both $^1(\pi\pi^*)$ and $^1(n_\pi\sigma^*)$ transitions are energetically accessible, the efficient S_1/S_2 vibronic coupling should facilitate the S–D bond dissociation reaction.

The kinetic energy distribution originating mainly from the $^1(\pi\pi^*)$ transition shows a Gaussian-like shape both for the upper
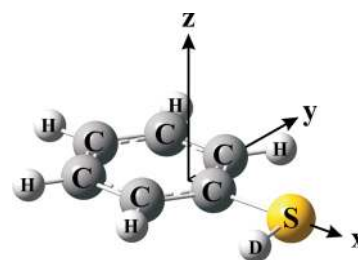

Figure 6. Cartesian coordinate used for the calculation of the transition dipole moment.

and the lower states of the phenylthiyl radical, which is quite different from that observed at 243 nm (Figures 3 and 5). This should result from the different shape of the exit potential energy surface along the S–D elongation at 266 nm from that at 243 nm not only in terms of energetics involved but also in terms of the multidimensional nature of the potential energy surface. The fraction going into the translational energy of fragments (f_T) for $C_6H_5S\cdot$ ($\tilde{X}$) at 266 nm is about 47% of the total available energy, which is much smaller than $f_T \sim 81\%$ for the $\tilde{X}$ state of phenylthiyl at 243 nm. This suggests that the vibrational excitation of thiophenol at 266 nm through the $^1(\pi\pi^*)$ transition, prior to be coupled to S_2 for the fast S–D bond dissociation, is quite significant compared to that at 243 nm. It is noteworthy that the shape of the kinetic energy release for the $\tilde{A}$ state channel is very similar to that for the $\tilde{X}$ state channel. This could be indicative of the fact that, once the vibrational content of the reactive flux is determined in the S_2/S_1 coupling region, it is maintained through the ultrafast passage over the S_2/S_0 conical intersection leading to final fragments. As the Ashfold group has pointed out in their study of phenol, the out-of-plane mode may be actively involved in the S_2/S_1 coupling because of the symmetry conservation.[1,2] The energy resolution of the present imaging setup, however, is not sufficient to identify the mode excited in the phenylthiyl radical. The phase space reached by the optical excitation (Franck–Condon region) followed by the efficient S_2/S_1 coupling should then be the dominant factor in determining product-state distributions. The branching ratio of $\tilde{A}$ to $\tilde{X}$ at 266 nm for the $^1(\pi\pi^*)$ transition is estimated to be $\sim$1.2, indicating that the wavepacket passage on the adiabatic potential energy surface leading to the $\tilde{A}$ phenylthiyl is slightly more efficient than that of the $\tilde{X}$ state. This is not much different from the branching ratio observed at 243 nm (vide supra),
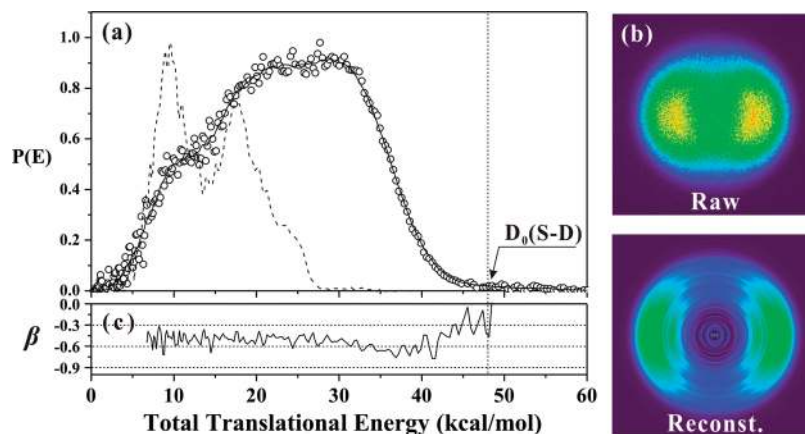
Figure 7. (a) Total translation energy distribution (○) of the fragmented D atom at 224 nm deduced from (b) raw and reconstructed images. Two shoulders at the low translational energy region could be due to the D distribution from the 266 nm photodissociation (dots). (c) Anisotropy parameter is plotted as a function of total translational energy.

consistent with the idea that the $\tilde{X}/\tilde{A}$ branching ratio is determined at the S_2/S_0 conical intersection.

The translational energy distribution from the 224 nm photodissociation is shown in Figure 7. Experimentally, it turns out to be nontrivial to get the D^+ image only from the 224 nm excitation since the ion signal decreases very sharply upon decreasing the counter-propagating 266 nm laser intensity used for the Doppler-reduced D fragment ionization. Therefore, the distribution in Figure 7 is likely to contain substantial contributions from the 266 nm photodissociation. Since the pump energy of 224 nm is quite high compared to the $\tilde{A}-\tilde{X}$ energy gap of the phenylthiyl radical, there is no discernible features which can be distinctly attributed to the ground and excited fragments. The anisotropy parameter is measured to be in the range from -0.5 to -0.7, indicating that the reaction is prompt at 224 nm. The transition dipole moment calculation associated with the 224 nm excitation will aid the interpretation of the experiment. It should be noted that the H-atom Rydberg tag translational spectroscopic study of thiophenol has been recently reported by Divine et al.[79] Major findings in ref 79 are quite consistent with those of our previous publications and this work, though some of the electronic transition assignments are in discrepancy. For instance, Divine et al. claimed that a switch from $^1(\pi\pi^*)$ to $^1(n_\pi\sigma^*)$ transitions occurs at the excitation wavelength of 275 nm based on the abrupt change of the anisotropy parameter observed around this energy. According to ref 79, the 266 nm excitation is thus entirely due to the $^1(n_\pi\sigma^*)$ transition. However, our experimental and theoretical findings here indicate that the absorption of the 266 nm excitation is mainly ascribed to $^1(\pi\pi^*)$ transition, whereas the contribution of $^1(n_\pi\sigma^*)$ seems to be minor (vide supra).

IV. Conclusion

We present here the study of photodissociation dynamics of thiophenol-d_1 at several different excitation wavelengths. While the thiophenol molecule is excited to the repulsive S_2 and higher-lying S_3 states at the 243 nm excitation, it is mainly prepared in the S_1 state at 266 nm with the small contribution of the S_2 state. The translational energy distribution at 266 nm is found to be very different from that observed at 243 nm, indicating that the S–D bond dissociation paths from initial S_1 and S_2/S_3 states are quite unique. The energy partitioning to the translational energy is 81% and 47% for the dissociation at 243 and 266 nm, respectively. The vibrational excitation of the phenylthiyl radical is more enhanced at 266 nm than it is for the

243 nm dissociation, giving a Gaussian-shaped distribution for both channels leading to $\tilde{X}$ and $\tilde{A}$ states of the fragment. An efficient vibronic coupling between repulsive S_2 and bound S_1 should be responsible for the ultrafast and yet vibrationally exciting fragmentation process at 266 nm. Ab initio calculations confirm the spectral assignment and identify molecular orbitals involved in the optical excitations. The present experimental work provides some important clues for the characteristic of the potential energy surfaces governing reaction dynamics especially on S_2/S_1 and S_2/S_0 conical intersections. Construction of multidimensional potential energy surfaces would be highly desirable for the thorough understanding of the thiophenol dissociation dynamics.

References and Notes

(1) Ashfold, M. N. R.; Cronin, B.; Devine, A. L.; Dixon, R. N.; Nix, M. G. D. *Science* **2006**, *312*, 1637.

(2) Nix, M. G. D.; Devine, A. L.; Ashfold, M. N. R.; Cronin, B.; Dixon, R. N. *J. Chem. Phys.* **2006**, *125*, 133318.

(3) Tseng, C.-M.; Lee, Y. T.; Ni, C.-K. *J. Chem. Phys.* **2004**, *121*, 2459.

(4) Sobolewski, A. L.; Domcke, W.; Dedonder-Lardeux, C.; Jouvet, C. *Phys. Chem. Chem. Phys.* **2004**, *4*, 1093.

(5) Lan, Z.; Domcke, W.; Vallet, V.; Soboleski, A. L.; Mahapatra, S. *J. Chem. Phys.* **2005**, *122*, 224315.

(6) Abe, M.; Ohtsuki, Y.; Fujimura, Y.; Lan, Z.; Domcke, W. *J. Chem. Phys.* **2006**, *124*, 224316.

(7) Lim, J. S.; Lim, I. S.; Lee, K.-S.; Ahn, D.-S.; Lee, Y. S.; Kim, S. K. *Angew. Chem., Int. Ed.* **2006**, *45*, 6290.

(8) Lim, I. S.; Lim, J. S.; Lee, Y. S.; Kim, S. K. *J. Chem. Phys.* **2007**, *126*, 034306.

(9) Lim, J. S.; Lee, Y. S.; Kim, S. K. *Angew. Chem., Int. Ed.* **2008**, *47*, 1853.

(10) Blank, D. A.; North, S. W.; Lee, Y. T. *Chem. Phys.* **1994**, *187*, 35.

(11) Wei, J.; Kuczmann, A.; Riedel, J.; Renth, R.; Temps, F. *Phys. Chem. Chem. Phys.* **2003**, *5*, 315.

(12) Lippert, H.; Ritze, H.-H.; Hertel, I. V.; Radloff, W. *ChemPhysChem* **2004**, *5*, 1423.

(13) Wei, J.; Riedel, J.; Kuczmann, A.; Renth, R.; Temps, F. *Faraday Discuss.* **2004**, *127*, 267.

(14) Cronin, B.; Nix, M. G. D.; Qadiri, R. H.; Ashfold, M. N. R. *Phys. Chem. Chem. Phys.* **2004**, *6*, 5031.

(15) van den Brom, A. J.; Kapelios, K.; Kitsopoulos, T. N.; Nahler, N. H.; Cronin, B.; Ashfold, M. N. R. *Phys. Chem. Chem. Phys.* **2005**, *7*, 892.

(16) Cronin, B.; Devine, A. L.; Nix, M. G. D.; Ashfold, M. N. R. *Phys. Chem. Chem. Phys.* **2006**, *8*, 3440.

(17) Cronin, B.; Nix, M. G. D.; Devine, A. L.; Dixon, R. N.; Ashfold, M. N. R. *Phys. Chem. Chem. Phys.* **2006**, *8*, 599.

(18) Vallet, V.; Lan, Z.; Mahapatra, S.; Soboleski, A. L.; Domcke, W. *Faraday Discuss.* **2004**, *127*, 283.

(19) Vallet, V.; Lan, Z.; Mahapatra, S.; Soboleski, A. L.; Domcke, W. *J. Chem. Phys.* **2005**, *123*, 144307.

(20) Barbatti, M.; Vazdar, M.; Aquino, A. J. A.; Eckert-Maksić, M.; Lischka, H. *J. Chem. Phys.* **2005**, *125*, 164323.

(21) Devine, A. L.; Cronin, B.; Nix, M. G. D.; Ashfold, M. N. R. *J. Chem. Phys.* **2006**, *125*, 184302.

(22) Dian, B. C.; Longarte, A.; Zwier, T. S. *J. Chem. Phys.* **2003**, *118*, 2696.

(23) Lin, M.-F.; Tseng, C.-M.; Lee, Y. T.; Ni, C. K. *J. Chem. Phys.* **2005**, *123*, 124303.

(24) Nix, M. G. D.; Devine, A. L.; Cronin, B.; Ashfold, M. N. R. *Phys. Chem. Chem. Phys.* **2006**, *8*, 2610.

(25) Sobolewski, A. L.; Domcke, W. *Chem. Phys. Lett.* **1999**, *315*, 293.

(26) Dedoner-Lardeux, C.; Jouvet, C.; Perun, S.; Sobolewski, A. L. *Phys. Chem. Chem. Phys.* **1999**, *5*, 293.

(27) Kang, H.; Lee, K. T.; Jung, B.; Ko, Y. J.; Kim, S. K. *J. Am. Chem. Soc.* **2002**, *124*, 12958.

(28) Canuel, C.; Mons, M.; Piuzzi, F.; Tardivel, B.; Dimicoli, I.; Elhanine, M. *J. Chem. Phys.* **2005**, *122*, 074316.

(29) Ullrich, S.; Schultz, T.; Zgierski, M. Z.; Stolow, A. *Phys. Chem. Chem. Phys.* **2004**, *6*, 2796.

(30) Matsika, S. S. *J. Phys. Chem. A* **2005**, *109*, 7538.

(31) Cohen, B.; Hare, P. M.; Kohler, B. *J. Am. Chem. Soc.* **2003**, *125*, 13594.

(32) Kang, H.; Jung, B.; Kim, S. K. *J. Chem. Phys.* **2003**, *118*, 6717.

(33) Ullrich, S.; Schultz, T.; Zgierski, M. Z.; Stolow, A. *J. Am. Chem. Soc.* **2004**, *126*, 2262.

(34) Zierhut, M.; Fischer, I. *Phys. Chem. Chem. Phys.* **2004**, *6*, 5178.

(35) Hünig, I.; Plützer, C.; Seefeld, K. A.; Löwenich, D.; Nispel, M.; Kleinermanns, K. *ChemPhysChem* **2005**, *5*, 1427.

(36) Nix, M. G. D.; Devine, A. L.; Cronin, B.; Ashfold, M. N. R. *J. Chem. Phys.* **2007**, *126*, 124312.

(37) Perun, S.; Sobolewski, A. L.; Domcke, W. *Chem. Phys.* **2005**, *313*, 107.

(38) Marian, C. M. *J. Chem. Phys.* **2005**, *122*, 104314.

(39) Blancafort, L. *J. Am. Chem. Soc.* **2006**, *128*, 210.

(40) Yamazaki, S.; Kato, S. *J. Am. Chem. Soc.* **2007**, *129*, 2910.

(41) Nielsen, S. B.; Sølling, T. I. *ChemPhysChem* **2005**, *6*, 1267.

(42) Chung, W. C.; Lan, Z.; Ohtsuki, Y.; Shimakura, N.; Domcke, W.; Fujimura, Y. *Phys. Chem. Chem. Phys.* **2007**, *9*, 2075.

(43) Hare, P. M.; Crespo-Hernández, C. E.; Kohler, B. *Proc. Natl. Acad. Sci.* **2007**, *104*, 435.

(44) He, Y.; Wu, C.; Kong, W. *J. Phys. Chem. A* **2003**, *107*, 5145.

(45) Zgierski, M. Z.; Patchkovskii, S.; Fujiwara, T.; Lim, E. C. *J. Phys. Chem. A* **2005**, *109*, 9384.

(46) Gustavsson, T.; Bányász, A.; Lazzarotto, E.; Markovitsi, D.; Scalmani, G.; Frisch, M. J.; Barone, V.; Improta, R. *J. Am. Chem. Soc.* **2006**, *128*, 607.

(47) Schneider, M.; Schon, C.; Fischer, I.; Rubio-Lago, L.; Kitsopoulos, T. *Phys. Chem. Chem. Phys.* **2007**, *9*, 6021.

(48) Matsika, S. *J. Phys. Chem. A* **2004**, *108*, 7584.

(49) Santoro, F.; Barone, V.; Gustavsson, T.; Improta, R. *J. Am. Chem. Soc.* **2006**, *128*, 16312.

(50) Schneider, M.; Maksimenka, R.; Buback, F. J.; Kitsopoulos, T.; Lago, L. R.; Fischer, I. *Phys. Chem. Chem. Phys.* **2006**, *8*, 3017.

(51) Perun, S.; Sobolewski, A. L.; Domcke, W. *J. Phys. Chem. A* **2006**, *110*, 13238.

(52) Talbot, F. O.; Tabarin, T.; Antoine, R.; Broyer, M.; Dugourd, P. *J. Chem. Phys.* **2005**, *122*, 074310.

(53) Kang, H.; Dedonder-Lardeux, C.; Jouvet, C.; Martrenchard, S.; Grégoire, G.; Desfrançois, C.; Schermann, J.-P.; Barat, M.; Fayeton, J. A. *Phys. Chem. Chem. Phys.* **2006**, *6*, 2628.

(54) Lepère, V.; Lucas, B.; Barat, M.; Fayeton, J. A.; Picard, V. J.; Jouvet, C.; Çarçabal, P.; Nielsen, I.; Dedonder-Lardeux, C.; Grégoire, G.; Fuiji, A. *J. Chem. Phys.* **2007**, *127*, 134313.

(55) Gregoire, G.; Jouvet, C.; Dedonder, C.; Sobolewski, A. L. *Chem. Phys.* **2006**, *324*, 398.

(56) Gregoire, G.; Jouvet, C.; Dedonder, C.; Sobolewski, A. L. *J. Am. Chem. Soc.* **2007**, *129*, 6223.

(57) Pino, G. A.; Dedonder-Lardeux, C.; Grégoire, G.; Jouvet, C.; Martrenchard, S.; Solgadi, D. *J. Chem. Phys.* **1999**, *111*, 10747.

(58) Pino, G. A.; Grégoire, G.; Dedonder-Lardeux, C.; Jouvet, C.; Martrenchard, S.; Solgadi, D. *Phys. Chem. Chem. Phys.* **2000**, *2*, 893.

(59) Grégoire, G.; Dedonder-Lardeux, C.; Jouvet, C.; Martrenchard, S.; Solgadi, D. *J. Phys. Chem. A* **2001**, *105*, 5971.

(60) Ishiuchi, S.; Daigoku, K.; Saeki, M.; Sakai, M.; Hashimoto, K.; Fujii, M. *J. Chem. Phys.* **2002**, *117*, 7077.

(61) Daigoku, K.; Ishiuchi, S.; Sakai, M.; Fujii, M.; Hashimoto, K. *J. Chem. Phys.* **2003**, *119*, 5149.

(62) Ishiuchi, S.; Sakai, M.; Daigoku, K.; Hashimoto, K.; Fujii, M. *J. Chem. Phys.* **2007**, *127*, 234304.

(63) Sobolewski, A. L.; Domcke, W. *J. Phys. Chem. A* **2001**, *105*, 9275.

(64) Macleod, N. A.; Simons, J. P. *Phys. Chem. Chem. Phys.* **2003**, *5*, 1123.

(65) Stert, V.; Hesse, L.; Lippert, H.; Schulz, C. P.; Radloff, W. *J. Phys. Chem. A* **2002**, *106*, 5051.

(66) Lippert, H.; Stert, V.; Hesse, L.; Schulz, C. P.; Hertel, I. V.; Radloff, W. *J. Phys. Chem. A* **2003**, *107*, 8239.

(67) Lippert, H.; Stert, V.; Hesse, L.; Schulz, C. P.; Hertel, I. V.; Radloff, W. *Chem. Phys. Lett.* **2003**, *376*, 40.

(68) David, O.; Dedonder-Lardeux, C.; Jouvet, C.; Kang, H.; Martrenchard, S.; Ebata, T.; Sobolewski, A. L. *J. Chem. Phys.* **2004**, *120*, 10101.

(69) Nam, S. H.; Park, H. S.; Song, J. K.; Park, S. M. *J. Phys. Chem. A* **2007**, *111*, 3480.

(70) Lee, K.-S.; Lim, J. S.; Ahn, D. S.; Choi, K.-W.; Kim, S. K.; Choi, Y. S. *J. Chem. Phys.* **2006**, *124*, 124307.

(71) Huang, C.; Li, W.; Kim, M. H.; Suits, A. G. *J. Chem. Phys.* **2006**, *125*, 12101.

(72) Dribinski, V.; Ossadtch, A.; Mandelshtam, V. A.; Reisler, H. *Rev. Sci. Instrum.* **2002**, *73*, 2634.

(73) Garcia, G. A.; Nahon, L.; Powis, I. *Rev. Sci. Instrum.* **2004**, *75*, 4989.

(74) Petiau, M.; Fabian, J.; Rosmus, P. *Phys. Chem. Chem. Phys.* **1999**, *1*, 5547.

(75) Petiau, M.; Fabian, J. *THEOCHEM* **2001**, *538*, 253.

(76) Frisch, M. J.; Trucks, G. W.; Schlegel, H. B.; Scuseria, G. E.; Robb, M. A.; Cheeseman, J. R.; Montgomery, J. A., Jr.; Vreven, T.; Kudin, K. N.; Burant, J. C.; Millam, J. M.; Iyengar, S. S.; Tomasi, J.; Barone, V.; Mennucci, B.; Cossi, M.; Scalmani, G.; Rega, N.; Petersson, G. A.; Nakatsuji, H.; Hada, M.; Ehara, M.; Toyota, K.; Fukuda, R.; Hasegawa, J.; Ishida, M.; Nakajima, T.; Honda, Y.; Kitao, O.; Nakai, H.; Klene, M.; Li, X.; Knox, J. E.; Hratchian, H. P.; Cross, J. B.; Bakken, V.; Adamo, C.; Jaramillo, J.; Gomperts, R.; Stratmann, R. E.; Yazyev, O.; Austin, A. J.; Cammi, R.; Pomelli, C.; Ochterski, J. W.; Ayala, P. Y.; Morokuma, K.; Voth, G. A.; Salvador, P.; Dannenberg, J. J.; Zakrzewski, V. G.; Dapprich, S.; Daniels, A. D.; Strain, M. C.; Farkas, O.; Malick, D. K.; Rabuck, A. D.; Raghavachari, K.; Foresman, J. B.; Ortiz, J. V.; Cui, Q.; Baboul, A. G.; Clifford, S.; Cioslowski, J.; Stefanov, B. B.; Liu, G.; Liashenko, A.; Piskorz, P.; Komaromi, I.; Martin, R. L.; Fox, D. J.; Keith, T.; Al-Laham, M. A.; Peng, C. Y.; Nanayakkara, A.; Challacombe, M.; Gill, P. M. W.; Johnson, B.; Chen, W.; Wong, M. W.; Gonzalez, C.; Pople, J. A. Gaussian 03, revision C.02; Gaussian, Inc.: Wallingford, CT, 2004.

(77) Werner, H. J.; Knowles, P. J.; Amos, R. D. et al. MOLPRO, version 2002.1, Birmingham, UK, 2002.

(78) Varsányi, G. *Assignments for Vibrational Spectra of 700 Benzene Derivatives*; Wiley: New York, 1974.

(79) Devine, A. L.; Nix, M. G. D.; Dixon, R. N.; Ashfold, M. N. R. *J. Phys. Chem. A* **2008**, *112*, 9563.